Journal of Alloys and Compounds 588 (2014) 17–24

Contents lists available at ScienceDirect

Journal of Alloys and Compounds

journal homepage: www.elsevier.com/locate/jalcom

Letter

A novel spherically porous Zr-doped spinel lithium titanate ($Li_4Ti_{5-x}Zr_xO_{12}$) for high rate lithium ion batteries

Xing Li [a,b,*], Shuihua Tang [a,b], Meizhen Qu [c], Pengxiao Huang [b], Wen Li [c], Zuolong Yu [c]

[a] State Key Laboratory of Oil and Gas Reservoir Geology and Exploitation, Southwest Petroleum University, Chengdu 610500, China
[b] School of Materials Science and Engineering, Southwest Petroleum University, Chengdu 610500, China
[c] Chengdu Institute of Organic Chemistry, Chinese Academy of Science, Chengdu 610041, China

ARTICLE INFO

Article history:
Received 25 September 2013
Received in revised form 7 November 2013
Accepted 8 November 2013
Available online 21 November 2013

Keywords:
Lithium-ion battery
Spinel lithium titanate
Spherically porous particle
Zr-doping

ABSTRACT

Spinel $Li_4Ti_5O_{12}$ has been demonstrated as a potential candidate for the anode material in lithium ion batteries because it has some unique characteristics as compared with carbon based anode materials. However, $Li_4Ti_5O_{12}$ has rather low electronic conductivity and only a moderate Li^+ diffusion coefficient, which make it suffer from the problem of poor rate capability. In the present study, novel spherically porous Zr-doped $Li_4Ti_{5-x}Zr_xO_{12}$ (x = 0.05, 0.1 and 0.2) anode materials were synthesized by using a rheological phase in combination with a spray drying reaction route, and their electrochemical properties between 0 V and 3 V were investigated. The results reveal that the spherically porous Zr-doped $Li_4Ti_{5-x}Zr_xO_{12}$ samples have better electrochemical performances than that of the pristine $Li_4Ti_5O_{12}$ without Zr-doping, but too great an amount of Zr-doping is disadvantageous. The $Li_4Ti_{4.9}Zr_{0.1}O_{12}$ exhibits the best rate capability and cycling stability among the Zr-doped samples. At the charge–discharge rate of 0.2 C, 5.0 C and 10.0 C between 0 V and 3 V, its initial discharge specific capacities were 308 mA h/g, 229 mA h/g and 210 mA h/g, respectively. After 50 cycles at 3.0 C, it remained at 201 mA h/g. Moreover, below 1.0 V there are no obviously irreversible reduction peaks in the CV curves of spherically porous Zr-doped $Li_4Ti_{5-x}Zr_xO_{12}$ electrodes even in the first cycle, which indicates that the electrolyte would not be reduced on the surfaces of Zr-doped $Li_4Ti_{5-x}Zr_xO_{12}$ electrodes below 1.0 V. Therefore, there would be less gas generation of the lithium ion battery while using the Zr-doped $Li_4Ti_{5-x}Zr_xO_{12}$ as the anode electrode.

1. Introduction

Recently, Spinel $Li_4Ti_5O_{12}$ has been demonstrated as a potential candidate for the anode material of lithium ion batteries for some of its unique characteristics as compared with carbon based anode materials [1–3]. It has good structural stability with an almost negligible volume change during the Li^+ insertion and extraction processes, which suggests a virtually unlimited cycle life [4–6]. It features a flat operating voltage plateau at around 1.55 V (vs. Li/Li^+), which can effectively prevent safety problems associated with carbon-based anode materials for the operating voltage is higher than the reduction potential of most organic electrolyte solvents [7–9]. These characteristics indicate that $Li_4Ti_5O_{12}$ is much safer and more stable than carbon based materials. Spinel $Li_4Ti_5O_{12}$ has been regarded as a good candidate material for negative electrodes used in long-life lithium-ion power batteries and large-scale long-life energy storage batteries [10].

However, $Li_4Ti_5O_{12}$ has rather low electronic conductivity (ca. 10^{-13} S cm^{-1}) and only a moderate Li^+ diffusion coefficient (10^{-9}–10^{-13} cm^2 S^{-1}) [11–15], which make it suffer from the problem of poor rate capability. In order to overcome the low electrical conductivity and further improve the rate capability of the $Li_4Ti_5O_{12}$, extensive work has previously been devoted. One approach is preparation of submicron or nanosized $Li_4Ti_5O_{12}$ because the smaller particle size can reduce the distance for lithium ion diffusion and provide for a higher electrode/electrolyte contact surface area, which is favorable to improve the electronic conductivity of this material [16–22]. Another is to synthesize $Li_4Ti_5O_{12}$ with ion doping for the doping can increase the amount of mixing Ti^{3+}/Ti^{4+} as charge compensation and thus enhance the electronic conductivity of $Li_4Ti_5O_{12}$, such as doping $Li_4Ti_5O_{12}$ with Ca^{2+} or Al^{3+} on the Li^+ sites [23–25], doping Ni^{2+} or W^{6+} on Ti^{4+} sites [26,27] and doping F^- on O^{2-} sites [28]. In addition, via forming composites of $Li_4Ti_5O_{12}$ and conductive second phases can also improve the surface electronic conductivity and further improve the rate capability of $Li_4Ti_5O_{12}$. The conductive second phases include

* Corresponding author at: State Key Laboratory of Oil and Gas Reservoir Geology and Exploitation, Southwest Petroleum University, Chengdu 610500, China. Tel./fax: +86 28 83032879.
E-mail address: lixing@swpu.edu.cn (X. Li).

0925-8388/$ - see front matter © 2013 Elsevier B.V. All rights reserved.
http://dx.doi.org/10.1016/j.jallcom.2013.11.046

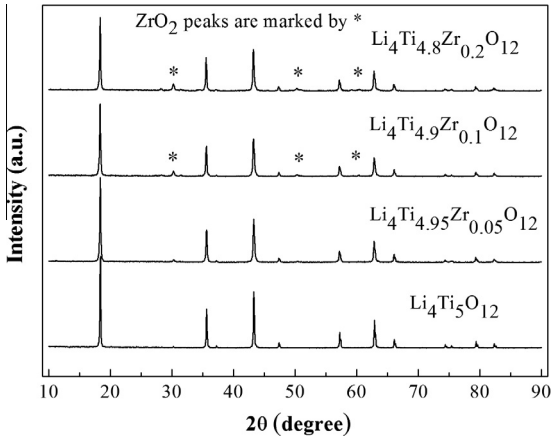

Fig. 1. X-ray diffraction patterns of the synthesized Zr-doped $Li_4Ti_{5-x}Zr_xO_{12}$ (x = 0.05, 0.1, 0.2) and the pristine $Li_4Ti_5O_{12}$. The ZrO_2 impurity peaks are marked by asterisks.

Table 1
Lattice parameters of synthesized $Li_4Ti_{5-x}Zr_xO_{12}$ (x = 0, 0.05, 0.1, 0.2) samples.

Sample	$Li_4Ti_5O_{12}$	$Li_4Ti_{4.95}Zr_{0.05}O_{12}$	$Li_4Ti_{4.9}Zr_{0.1}O_{12}$	$Li_4Ti_{4.8}Zr_{0.2}O_{12}$
a (Å)	8.354	8.356	8.360	8.361

nobel metal (Ag, Au) [29,30], carbon [31–39] and graphene [40–45]. In our previous work, we studied the electrochemical performances of Zr-doped $Li_4Ti_5O_{12}$ in the form of $Li_4Ti_{5-x}Zr_xO_{12}$ (x = 0.05, 0.1 and 0.2) and found that Zr-doping obviously improved the rate capability of $Li_4Ti_5O_{12}$ via the generation of small particle size and less agglomeration [46]. In that work, however, the electrochemical performances of the $Li_4Ti_{5-x}Zr_xO_{12}$ samples were investigated only at the cut-off voltage of 1–3 V, and the electrochemical behaviors of the Zr-doped $Li_4Ti_{5-x}Zr_xO_{12}$ discharged to a low voltage of 0 V were not clear. Recently, some researchers have reported that $Li_4Ti_5O_{12}$ can be discharged to 0 V, which can improve the specific capacity and energy density and does not influence the cycling performance of the material [47–49].

In the present study, the Zr-doped $Li_4Ti_{5-x}Zr_xO_{12}$ (x = 0.05, 0.1 and 0.2) with spherically porous microstructure was prepared by a rheological phase in combination with a spray drying reaction route. The particle size, morphology and electrochemical performance of the $Li_4Ti_{5-x}Zr_xO_{12}$ at the cut-off voltage of 0–3 V were investigated. For comparison, pristine $Li_4Ti_5O_{12}$ without Zr-doping was also investigated at the cut-off voltage of 0–3 V.

2. Experimental

Samples of the spherically porous Zr-doped $Li_4Ti_{5-x}Zr_xO_{12}$ (x = 0.05, 0.1 and 0.2) were prepared by using a rheological phase in combination with a spray drying reaction route from $CH_3COOLi{\cdot}2H_2O$, TiO_2 and $Zr(NO_3)_4{\cdot}5H_2O$. A 0.2 mol% excessive $CH_3COOLi{\cdot}2H_2O$ was provided to compensate for Li volatilization during the high temperature heating. Firstly, the $CH_3COOLi{\cdot}2H_2O$, TiO_2 and $Zr(NO_3)_4{\cdot}5H_2O$ were added to distilled water and stirred magnetically to form a well-mixed precursor slurry. Then, a 1.7-MHz ultrasonic spray generator with six vibrators was used to turn the precursor slurry into a large amount of droplets, which were carried into the high temperature tubular reactor by a carrier gas. Finally, the precursor droplets were calcined in air atmosphere at 800 °C for 8 h to obtain the spherically porous $Li_4Ti_{5-x}Zr_xO_{12}$ samples. The pristine $Li_4Ti_5O_{12}$ sample without Zr-doping was also prepared using a similar rheological phase in combination with spray drying reaction route as mentioned above.

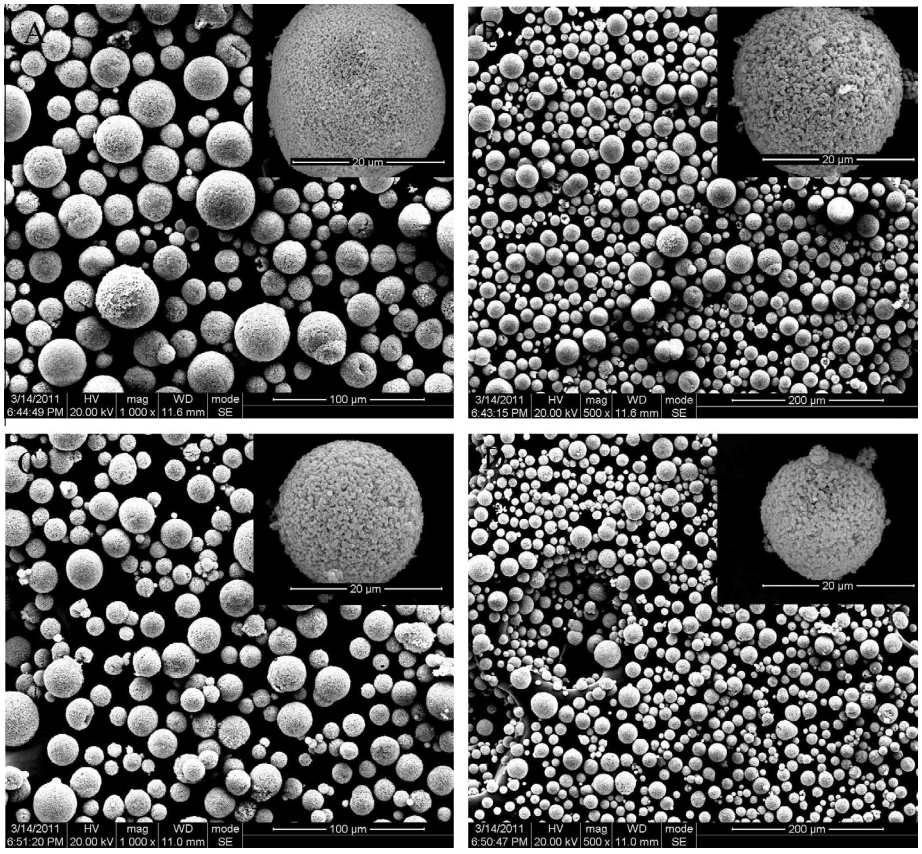

Fig. 2. SEM pictures of the $Li_4Ti_{5-x}Zr_xO_{12}$ (x = 0, 0.05, 0.1, 0.2) samples, from image A to image D is the pristine $Li_4Ti_5O_{12}$, $Li_4Ti_{4.95}Zr_{0.05}O_{12}$, $Li_4Ti_{4.9}Zr_{0.1}O_{12}$ and $Li_4Ti_{4.8}Zr_{0.2}O_{12}$ respectively.

The X-ray diffraction (XRD) patterns of the Zr-doped $Li_4Ti_{5-x}Zr_xO_{12}$ (x = 0.05, 0.1 and 0.2) and the pristine $Li_4Ti_5O_{12}$ were recorded using the Philips X' Pert Pro MPD DY1219 with a Cu Kα radiation source. Particle morphologies and sizes of the samples were observed by scanning electronic microscopy (SEM FEI INSPECT-F). Specific surface areas of the samples were evaluated via nitrogen adsorption/desorption at −196 °C using a Builder SSA-4200 apparatus. The electrochemical characterizations were measured by using two electrode coin-type half cells (CR2032). The $Li_4Ti_{5-x}Zr_xO_{12}$ (x = 0, 0.05, 0.1 and 0.2) electrodes were prepared by mixing 85 wt% of this active material, 10 wt% acetylene black (HaoChem Chemical), and 5 wt% LA-132 binder (Chengdu Indigo Power Sources Co., Ltd. LA132 is a kind of aqueous binder for the cathode or anode materials of lithium ion batteries, which has excellent anti-oxidation ability and anti-reducibility. The major constituents of the LA132 are acrylonitrile copolymer and water). The prepared paste was then spread onto copper foil using a doctor blade, with a 100 μm gap. The working electrodes were then dried at 80 °C in a vacuum for 16 h before cell assembly. Li metal was used as the counter and reference electrode, and Celgard 2400 was the separator. The electrolyte was 1 M $LiPF_6$/EC:DEC:DMC (1:1:1 in volume). The cells were assembled in a glove box filled with high purity argon gas. Galvanostatic discharge–charge measurements were performed at constant cut-off voltages of 0–3 V at room temperature (25 °C) using the Neware automatic batteries tester (Neware BTS, Shenzhen, China). Cyclic voltammograms were recorded from 0 V to 3 V with a scan rate of 0.2 mV/s by using the Autolab Pgstat302 N electrochemical workstation.

3. Results and discussion

The XRD patterns of the samples of Zr-doped $Li_4Ti_{5-x}Zr_xO_{12}$ (x = 0.05, 0.1 and 0.2) and the pristine $Li_4Ti_5O_{12}$ are shown in Fig. 1. It can be seen from Fig. 1 that the main phase of all investigated samples is $Li_4Ti_5O_{12}$ with a cubic spinel structure, which suggests that the dopant Zr does not obviously influence the formation of the spinel $Li_4Ti_5O_{12}$ during heat-treatment. However, from Fig. 1, it can be observed that the XRD peak intensities of the samples decrease with the increase of the amount of Zr, which suggests that the Zr-doped $Li_4Ti_5O_{12}$ samples have relatively poor crystallinity. The lattice parameters of the $Li_4Ti_{5-x}Zr_xO_{12}$ (x = 0, 0.05, 0.1 and 0.2) samples obtained according to the Rietveld method are shown in Table 1. It can be observed from Table 1 that the lattice parameter increases with the increased amount of dopant Zr, which indicates that some of the dopant Zr has entered the lattice structure of $Li_4Ti_5O_{12}$. This should be ascribable to the substitution of some Zr for Ti sites and to the fact that the size of the Zr^{4+} (0.080 nm) ion is larger than that of the Ti^{4+} (0.068 nm) ion. Furthermore, Fig. 1 shows that ZrO_2 impurity peaks are detected in the XRD patterns of the $Li_4Ti_{4.9}Zr_{0.1}O_{12}$ and $Li_4Ti_{4.8}Zr_{0.2}O_{12}$ samples and that the peak intensities of ZrO_2 increase with the increased amount of doping Zr, which suggests that some Zr cannot enter the lattice structure of the $Li_4Ti_5O_{12}$ as the dopant amount increases. In this article, the ZrO_2 impurity peaks in the X-ray diffraction patterns are marked by asterisks.

Fig. 2 shows the SEM pictures of the $Li_4Ti_{5-x}Zr_xO_{12}$ (x = 0, 0.05, 0.1 and 0.2) samples. Image A is the pristine $Li_4Ti_5O_{12}$ sample without Zr-doping, images B, C and D are the Zr-doped $Li_4Ti_{5-x}Zr_xO_{12}$ (x = 0.05, 0.1, 0.2) samples respectively. From image A to image D, it can be observed that all the samples that prepared by rheological phase in combination with spray drying have spherically porous microstructure. The particles size of the spherically porous $Li_4Ti_{5-x}Zr_xO_{12}$ (x = 0, 0.05, 0.1 and 0.2) samples is about 15–20 μm, and there are almost no obviously difference of the spherically porous particles of the samples with and without Zr-doping. These suggest that using a rheological phase in combination with a spray drying reaction route is suitable to prepare spherical microstructure, and the porous microstructure of the particle should be due to the pyrolysis of the precursor [50].

Fig. 3 shows close-up SEM pictures of the $Li_4Ti_{5-x}Zr_xO_{12}$ (x = 0, 0.05, 0.1, 0.2) samples. It can be observed that the spherically porous particles of the samples (images A–D) are actually constituted by aggregations of smaller particulates with different size,

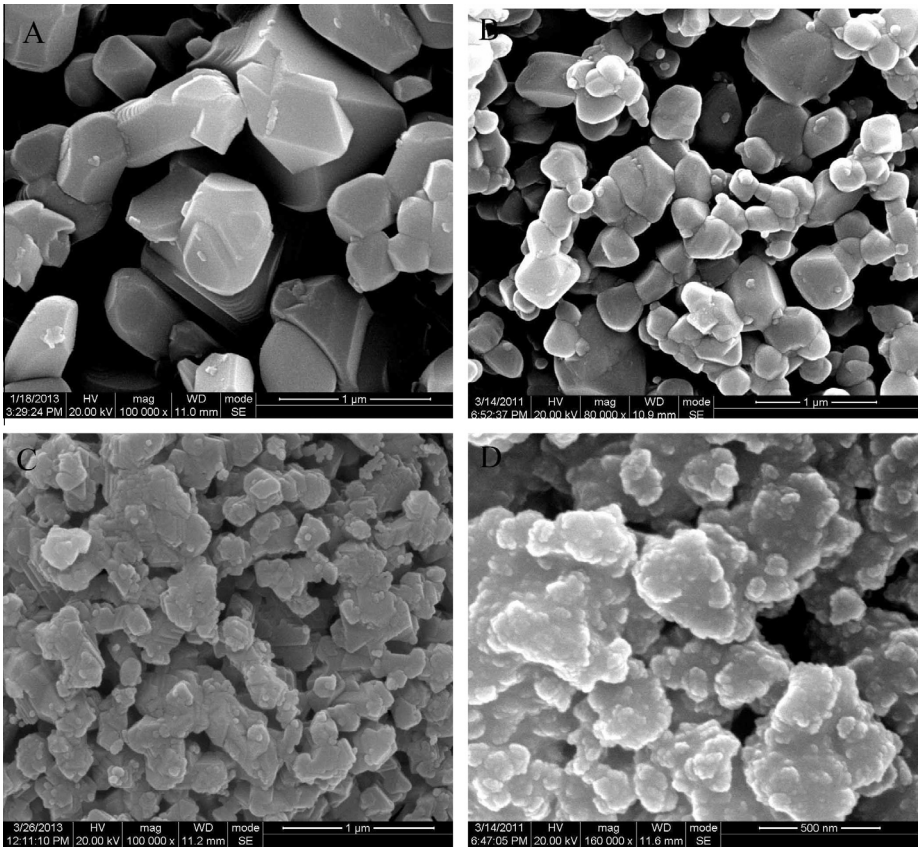

Fig. 3. Close-up SEM pictures of the $Li_4Ti_{5-x}Zr_xO_{12}$ (x = 0, 0.05, 0.1, 0.2) samples, from image A to image D is the pristine $Li_4Ti_5O_{12}$, $Li_4Ti_{4.95}Zr_{0.05}O_{12}$, $Li_4Ti_{4.9}Zr_{0.1}O_{12}$ and $Li_4Ti_{4.8}Zr_{0.2}O_{12}$ respectively.

furthermore, the particulates size of the $Li_4Ti_5O_{12}$ sample (image A) without Zr-doping is larger than that of the samples (images B–D) with Zr-doping. The particulates size as shown in image A is more than 500 nm, while the particulates size shown in images B–D is less than 300 nm and becomes smaller with the increased doping amount of Zr. These could be ascribed to the following reasons: (1) the rheological phase in combination with spray drying reaction route is favorable to prepare spherically porous microstructure that consisting of aggregations of smaller particulates; (2) the dopant Zr that could enter the lattice structure of the $Li_4Ti_5O_{12}$, resulting in lattice distortion and poor crystallinity, which hindered the particulate growth during heat-treatment; (3) part of the Zr dopant that could not enter the lattice structure of the $Li_4Ti_5O_{12}$ and constituted an impurity in the form of ZrO_2, which might likewise hindered undesirable particulate growth.

The BET surface areas of the Zr-doped $Li_4Ti_{5-x}Zr_xO_{12}$ (x = 0.05, 0.1, 0.2) and the pristine $Li_4Ti_5O_{12}$ samples were determined by a nitrogen adsorption method, as shown in Table 2. It can be observed that the Zr-doped $Li_4Ti_{5-x}Zr_xO_{12}$ samples have larger BET surface areas than the pristine $Li_4Ti_5O_{12}$ sample without Zr-doping and the BET surface areas of the Zr-doped samples increase with the increased doping amount of Zr. This also suggests that the size of the particulate consisted in the spherically porous microstructure of the pristine $Li_4Ti_5O_{12}$ is larger than that of the Zr-doped $Li_4Ti_{5-x}Zr_xO_{12}$ and the particulates size of the doped samples decrease with the increased amount of Zr doping.

Table 2
BET surface areas of the $Li_4Ti_{5-x}Zr_xO_{12}$ (x = 0, 0.05, 0.1, 0.2) samples.

	$Li_4Ti_5O_{12}$	$Li_4Ti_{4.95}Zr_{0.05}O_{12}$	$Li_4Ti_{4.9}Zr_{0.1}O_{12}$	$Li_4Ti_{4.8}Zr_{0.2}O_{12}$
BET areas (m^2/g)	4.525	4.720	5.240	5.350

The tap densities of the $Li_4Ti_{5-x}Zr_xO_{12}$ (x = 0, 0.05, 0.1, 0.2) samples are about 1.2 g/cm^3. This is a quite high tap density, which indicates that using rheological phase in combination with spray drying reaction route to synthesize spherically porous particle is favorable to improve the tap density of the sample. And in fact, the high tap density is advantageous in practical application, which can increase the energy density of the battery.

Cyclic voltammograms of the electrodes of the pristine $Li_4Ti_5O_{12}$ and the Zr-doped $Li_4Ti_{5-x}Zr_xO_{12}$ (x = 0.05, 0.1, 0.2) at a scan rate of 0.2 mV/s between 0 V and 3 V are shown in Fig. 4. It is well known that the cathodic and anodic peaks of the $Li_4Ti_5O_{12}$ at about 1.75 V and 1.45 V are attributed to the redox of Ti^{4+}/Ti^{3+} and that the reduction and oxidation peaks below 1.0 V are caused by a multi step restore of Ti^{4+} [51]. From Fig. 4, it can be observed that all the investigated electrodes have similar redox peaks between 1 V and 3 V, but that below 1.0 V, only the $Li_4Ti_5O_{12}$ electrode shows obviously irreversible peaks that appear at around 0.62 V during the reduction process. The irreversible reduction peaks of the $Li_4Ti_5O_{12}$ electrode can be clearly seen in Fig. 5, which gives the close-up cyclic voltammograms of Fig. 4 between 0.4 V and 0.8 V. As shown in Fig. 5, moreover, the irreversible peak at around 0.62 V on the CV curves of the $Li_4Ti_5O_{12}$ electrode does not disappear from the second cycle. This indicates that the reduction decomposition reaction of the electrolyte continues to occur on the $Li_4Ti_5O_{12}$ electrode after the first cycle, and the SEI film formed on $Li_4Ti_5O_{12}$ particles which is not like that formed on the carbon anode cannot suppress the further reduction decomposition of the electrolyte. He et al. have reported that the reason for the

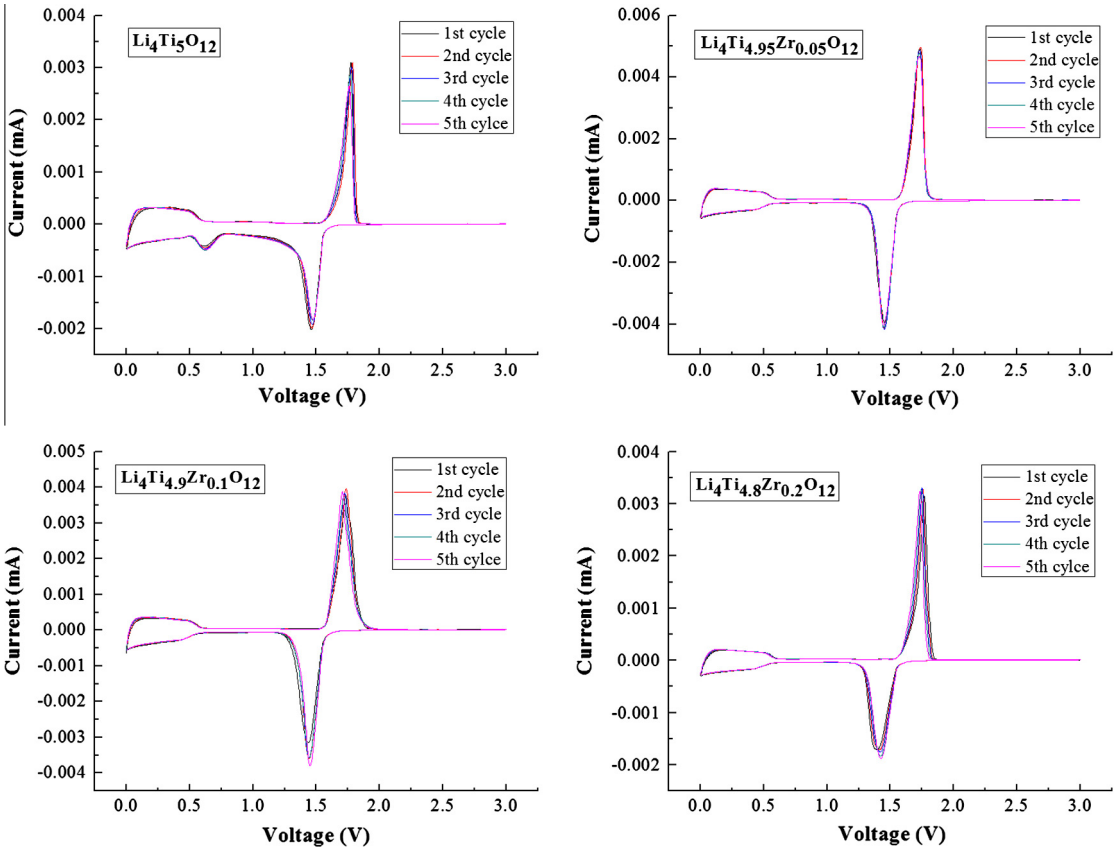

Fig. 4. Cyclic voltammograms of the pristine $Li_4Ti_5O_{12}$ electrode, $Li_4Ti_{4.95}Zr_{0.05}O_{12}$ electrode, $Li_4Ti_{4.9}Zr_{0.1}O_{12}$ electrode and $Li_4Ti_{4.8}Zr_{0.2}O_{12}$ electrode between 0 V and 3 V. Scan rate: 0.2 mV/s.

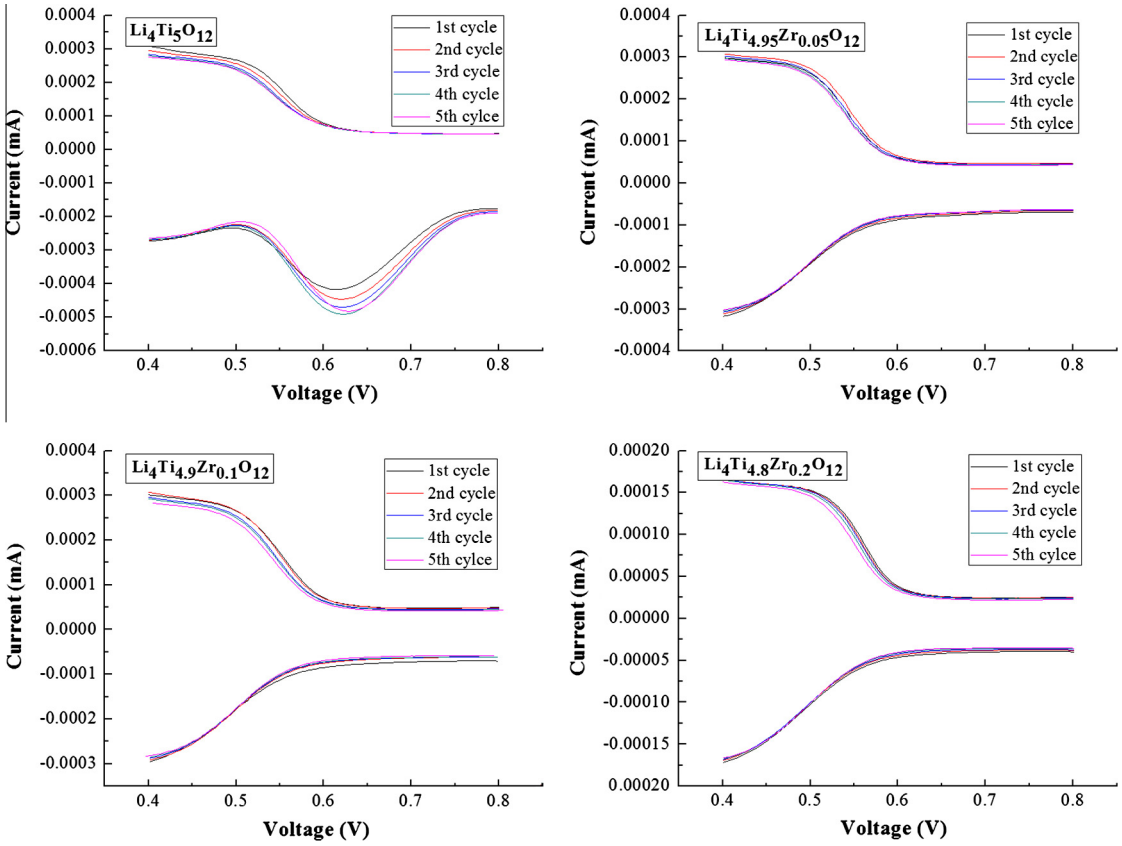

Fig. 5. Close-up cyclic voltammograms of the $Li_4Ti_5O_{12}$ electrode, $Li_4Ti_{4.95}Zr_{0.05}O_{12}$ electrode, $Li_4Ti_{4.9}Zr_{0.1}O_{12}$ electrode and $Li_4Ti_{4.8}Zr_{0.2}O_{12}$ electrode between 0.4 V and 0.8 V.

further reduction decomposition of the electrolyte occurred on the surface of the $Li_4Ti_5O_{12}$ particles could be ascribed to the possibility that the SEI film formed on the $Li_4Ti_5O_{12}$ particles may be thin and have rich pores, which cannot cover the catalytic active sites of $Li_4Ti_5O_{12}$ particles and separate the $Li_4Ti_5O_{12}$ particles from the electrolyte [52].

As shown in Figs. 4 and 5, below 1.0 V, it can be observed that even in the first cycle there are no obviously irreversible reduction peaks existing in the CV curves of Zr-doped $Li_4Ti_{5-x}Zr_xO_{12}$ ($x = 0.05$, 0.1, 0.2) electrodes. This indicates that the electrolyte would not be reduced on the surfaces of Zr-doped $Li_4Ti_{5-x}Zr_xO_{12}$ ($x = 0.05$, 0.1, 0.2) electrodes below 1.0 V, and there would be less gas generation of the lithium ion battery while using the Zr-doped $Li_4Ti_{5-x}Zr_xO_{12}$ ($x = 0.05$, 0.1, 0.2) as the anode electrode. He et al also reported that there are no irreversible reduction peaks below 1.0 V existing in the CV curves of the carbon coated $Li_4Ti_5O_{12}$ electrodes, however, the disappearance of the irreversible reduction peaks below 1.0 V of the carbon coated $Li_4Ti_5O_{12}$ electrode appeared from the second cycle [52]. The reason he gave for the phenomenon was that the carbon coating layer could form successive SEI film in the first cycle which covered the catalytic active sites of $Li_4Ti_5O_{12}$ particles and prevented the further reduction decomposition of electrolyte [53]. In our study, the reason that leading to the disappearance of the irreversible reduction peaks below 1.0 V of the Zr-doped $Li_4Ti_{5-x}Zr_xO_{12}$ ($x = 0.05$, 0.1, 0.2) electrodes is obviously different from the carbon coated $Li_4Ti_5O_{12}$ electrode. In the present work, the reason could be attributed to the possibility that the part of the Zr dopant that could not enter the lattice structure of the $Li_4Ti_5O_{12}$ and constituted an impurity in the form of ZrO_2 which covered the catalytic active sites of $Li_4Ti_5O_{12}$ particles and prevented the reduction decomposition of the electrolyte.

Table 3
Potential differences of the first cycle between anodic and cathodic peaks for the $Li_4Ti_5O_{12}$ electrode and the spherically porous Zr-doped $Li_4Ti_{5-x}Zr_xO_{12}$ ($x = 0.05$, 0.1, 0.2) electrodes.

Sample	Anodic peak (V)	Cathodic peak (V)	Potential difference (V)
$Li_4Ti_5O_{12}$	1.779	1.460	0.319
$Li_4Ti_{4.95}Zr_{0.05}O_{12}$	1.735	1.462	0.273
$Li_4Ti_{4.9}Zr_{0.1}O_{12}$	1.709	1.451	0.258
$Li_4Ti_{4.8}Zr_{0.2}O_{12}$	1.733	1.433	0.300

The potential differences of the first cycle between anodic and cathodic peaks of the pristine $Li_4Ti_5O_{12}$ electrode and the Zr-doped $Li_4Ti_{5-x}Zr_xO_{12}$ ($x = 0.05$, 0.1, 0.2) electrodes are shown in Table 3. It can be observed that the Zr-doped $Li_4Ti_{5-x}Zr_xO_{12}$ electrodes have lower potential differences than that of pristine $Li_4Ti_5O_{12}$ electrode, and the Zr-doped $Li_4Ti_{5-x}Zr_xO_{12}$ ($x = 0.1$) electrode has the smallest potential difference among the doped electrodes. This indicates that Zr-doping is favorable for reducing the electrodes polarization, but that too high an amount of doping is disadvantageous. This could be ascribed to the fact that Zr-doped $Li_4Ti_{5-x}Zr_xO_{12}$ samples have smaller particulates size, and the smaller particulates could reduce the distance for lithium ion diffusion and provide for a higher electrode/electrolyte contact surface area, which would improve the lithium ion conductivity and thus reduce the electrodes polarization.

Fig. 6 shows the cyclic performances of the pristine $Li_4Ti_5O_{12}$ and the Zr-doped $Li_4Ti_{5-x}Zr_xO_{12}$ ($x = 0.05$, 0.1, 0.2) samples at different rates from 0.2 C, 1.0 C, 3.0 C, 5.0 C to 10.0 C and then in returned from 10 C to 0.2 C between 0 V and 3 V. The charge–discharge processes of the samples were carried out for 5 cycles at

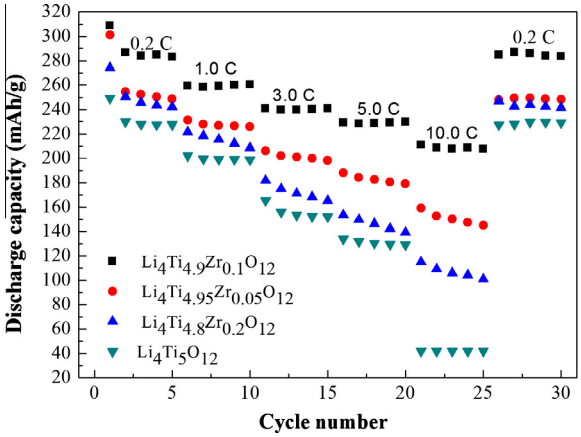

Fig. 6. Cyclic performances of the pristine $Li_4Ti_5O_{12}$, $Li_4Ti_{4.95}Zr_{0.05}O_{12}$, $Li_4Ti_{4.9}Zr_{0.1}O_{12}$ and $Li_4Ti_{4.8}Zr_{0.2}O_{12}$ samples between 0 V and 3 V at different rates: 1–5th cycles at 0.2 C, 6–10th at 1.0 C, 11–15th at 3.0 C, 16–20th at 5.0 C, 21–25th at 10.0 C and 26–30th at 0.2 C.

0.2 C, 1.0 C, 3.0 C, 5.0 C, 10.0 C and again at 0.2 C, respectively. It can be observed that the pristine $Li_4Ti_5O_{12}$ sample exhibited a lower discharge specific capacity as compared with the doped samples at different rates. At 0.2 C, its initial discharge specific capacity was 249 mA h/g, and at 1.0 C, its discharge capacity remained at 202 mA h/g. With the rate increase, however, its discharge specific capacity quickly decreased. At 3.0 C, its capacity was 165 mA h/g; at 5.0 C, it was 134 mA h/g; and at 10.0 C, its capacity remained at only about 42 mA h/g. In contrast, the Zr-doped $Li_4Ti_{5-x}Zr_xO_{12}$ ($x = 0.05, 0.1, 0.2$) samples displayed relatively higher discharge specific capacity at different rates, and the discharge capacities of the doped samples manifested less capacity degradation with the rate increase than the pristine $Li_4Ti_5O_{12}$. For example, at 0.2 C, the initial discharge specific capacities of the doped samples $Li_4Ti_{4.95}Zr_{0.05}O_{12}$, $Li_4Ti_{4.9}Zr_{0.1}O_{12}$, and $Li_4Ti_{4.8}Zr_{0.2}O_{12}$ were 308 mA h/g, 301 mA h/g, and 274 mA h/g, respectively; at 3.0 C, they were 240 mA h/g, 206 mA h/g and 182 mA h/g; and even at 10.0 C, they still remained at 210 mA h/g, 159 mA h/g and 115 mA h/g. For clear observation, the initial discharge capacities of the samples $Li_4Ti_5O_{12}$, $Li_4Ti_{4.95}Zr_{0.05}O_{12}$, $Li_4Ti_{4.9}Zr_{0.1}O_{12}$, and $Li_4Ti_{4.8}Zr_{0.2}O_{12}$ as a function of the charge/discharge rates are shown in Fig. 7. From Fig. 7, it can also be observed that the Zr-doped $Li_4Ti_{5-x}Zr_xO_{12}$ samples have higher discharge specific capacity and less capacity degradation at different rates than the pristine $Li_4Ti_5O_{12}$ sample. These results indicate that the Zr-doping could improve the capacity and rate capability of the $Li_4Ti_5O_{12}$. This could be ascribed to the fact that the Zr-doping samples have smaller particulates size than the pristine $Li_4Ti_5O_{12}$. Smaller particulates could reduce the distance for lithium-ion diffusion and provide for a higher electrode/electrolyte contact surface area, which would improve the lithium ion conductivity of the electrodes, resulting in good rate capability. Furthermore, the spherically porous microstructure of the Zr-doped samples was also favorable for improving the Li-ion diffusion and the contact surface areas between the electrodes and the electrolyte.

It is worth noting that, as shown in Fig. 6, the $Li_4Ti_{4.9}Zr_{0.1}O_{12}$ sample has the best rate capability of all the doped samples, which indicates that the $x = 0.1$ amount of dopant is appropriate. This result is in good agreement with the cyclic voltammograms of the Zr-doped $Li_4Ti_{5-x}Zr_xO_{12}$ ($x = 0, 0.05, 0.1, 0.2$) electrodes mentioned above, in which the $Li_4Ti_{4.9}Zr_{0.1}O_{12}$ electrode has the smallest potential difference. When returning to 0.2 C after the progressive rate tests, moreover, all the samples could recover their initial discharge capacity, which means that there was also almost no volume change during the lithium ion intercalation and deintercalation process between 0 V and 3 V.

Figs. 8 and 9 show the initial charge–discharge curves of the $Li_4Ti_{4.9}Zr_{0.1}O_{12}$ and $Li_4Ti_5O_{12}$ electrodes at the rate of 0.2 C, 1.0 C, 3.0 C, 5.0 C and 10.0 C respectively. There, it can be seen that the $Li_4Ti_{4.9}Zr_{0.1}O_{12}$ and $Li_4Ti_5O_{12}$ electrodes have similar charge–discharge plateaus, which also indicates that the Zr-doping did not affect the electrochemical reaction process of the $Li_4Ti_5O_{12}$. From Figs. 8 and 9, it can been observed that the $Li_4Ti_{4.9}Zr_{0.1}O_{12}$ and $Li_4Ti_5O_{12}$ electrodes both have two discharge plateaus at about 1.5 V and 0.6 V between 0 V and 3 V respectively, which indicates that the discharge specific capacities of the two electrodes are the result of two different electrochemical reaction processes. Furthermore, the margins between the charge and discharge plateau potentials of $Li_4Ti_{4.9}Zr_{0.1}O_{12}$ and $Li_4Ti_5O_{12}$ electrodes both become large with the increase of the charge–discharge rate. However, the margins of the $Li_4Ti_{4.9}Zr_{0.1}O_{12}$ electrode are obviously smaller than those of the $Li_4Ti_5O_{12}$ electrode at different rate. This means that the polarization of $Li_4Ti_{4.9}Zr_{0.1}O_{12}$ electrode is lower than that of $Li_4Ti_5O_{12}$, which should be ascribed to the smaller particulates size of the $Li_4Ti_{4.9}Zr_{0.1}O_{12}$ sample.

For evaluating the cycling stability of the $Li_4Ti_{4.9}Zr_{0.1}O_{12}$ sample, it was further charge–discharged at a current rate of 3 C for another 50 cycles after the 30 cycles electrochemical tests performed at 0.2 C, 1.0 C, 3.0 C, 5.0 C, 10.0 C and again at 0.2 C. For comparison, the pristine $Li_4Ti_5O_{12}$ sample was also tested under the same

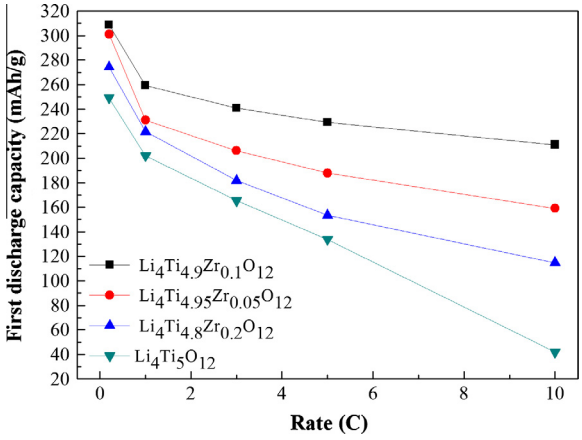

Fig. 7. Initial discharge capacities of the samples $Li_4Ti_5O_{12}$, $Li_4Ti_{4.95}Zr_{0.05}O_{12}$, $Li_4Ti_{4.9}Zr_{0.1}O_{12}$, and $Li_4Ti_{4.8}Zr_{0.2}O_{12}$ as a function of the charge/discharge rates.

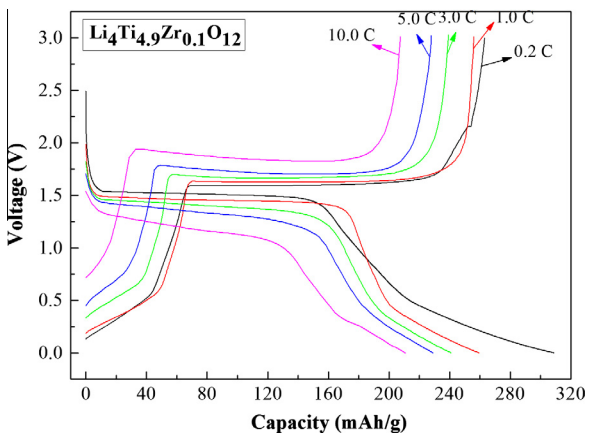

Fig. 8. Initial charge–discharge curves of the $Li_4Ti_{4.9}Zr_{0.1}O_{12}$ sample at the rate of 0.2 C, 1.0 C, 3.0 C, 5.0 C and 10.0 C between 0 V and 3 V, respectively.

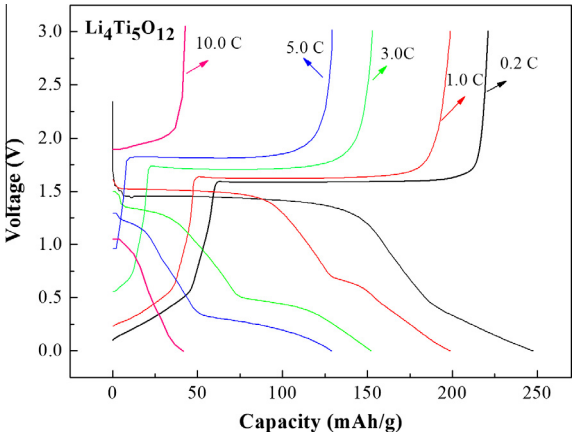

Fig. 9. Initial charge–discharge curves of the pristine $Li_4Ti_5O_{12}$ sample at the rate of 0.2 C, 1.0 C, 3.0 C, 5.0 C and 10.0 C between 0 V and 3 V, respectively.

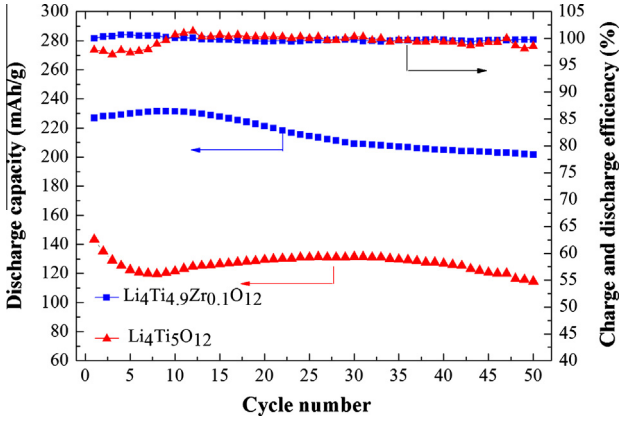

Fig. 10. Cyclic performances and charge–discharge efficiencies of the $Li_4Ti_{4.9}Zr_{0.1}O_{12}$ and pristine $Li_4Ti_5O_{12}$ samples at 3.0 C.

conditions. The results are shown in Fig. 10, where it can be observed that the $Li_4Ti_{4.9}Zr_{0.1}O_{12}$ sample shows a stable cycle life. The initial discharge specific capacity of the $Li_4Ti_{4.9}Zr_{0.1}O_{12}$ was 227 mAh/g, and after 50 charge–discharge cycles, its discharge capacity remained at 201 mAh/g. However, the pristine $Li_4Ti_5O_{12}$ sample shows a poor cycle life as compared with the $Li_4Ti_{4.9}Zr_{0.1}O_{12}$ sample. Its initial discharge specific capacity was 143 mAh/g, and after 50 cycles, its discharge capacity remained at only 114 mAh/g. Furthermore, as shown in Fig. 10, the charge and discharge efficiency of the $Li_4Ti_{4.9}Zr_{0.1}O_{12}$ sample is also better than that of pristine $Li_4Ti_5O_{12}$.

4. Conclusions

The Zr-doped $Li_4Ti_{5-x}Zr_xO_{12}$ ($x = 0.05$, 0.1, 0.2) samples were synthesized by using a rheological phase in combination with a spray drying reaction route and their structures and electrochemical characteristics between 0 V and 3 V were investigated in the present study. For comparison, the pristine $Li_4Ti_5O_{12}$ synthesized using a similar method was also investigated. The results show that all of the Zr-doped $Li_4Ti_{5-x}Zr_xO_{12}$ and the pristine $Li_4Ti_5O_{12}$ have spherically porous microstructures, and the spherically porous microstructures of the samples are actually constituted by aggregations of smaller particulates. However, the particulates of the Zr-doped $Li_4Ti_{5-x}Zr_xO_{12}$ samples are much smaller than that of the pristine $Li_4Ti_5O_{12}$ sample, and the particulates size of the Zr-doped samples gets smaller with the increase of Zr-doping. The smaller particulates could reduce the distance for lithium ion diffusion and provide for a higher electrode/electrolyte contact surface area, which resulted in the Zr-doped $Li_4Ti_{5-x}Zr_xO_{12}$ samples have better electrochemical performances than that of pristine $Li_4Ti_5O_{12}$. Furthermore, the spherically porous microstructure of the samples have a quite high tap density of about 1.2 g/cm^3, which is advantageous in practical application because the high tap density can increase the energy density of the battery. Moreover, the cyclic voltammograms of the Zr-doped $Li_4Ti_{5-x}Zr_xO_{12}$ electrodes show that there are no obviously irreversible reduction peaks existing below 1.0 V even in the first cycle, which indicates that the Zr-doped $Li_4Ti_{5-x}Zr_xO_{12}$ samples have a high practical application value for the electrolyte would not be reduced on the surfaces of the samples below 1.0 V.

Acknowledgements

This work was carried out with financial support from the National Natural Science Foundation of China (No. 51302232), the Ministry of Science and Technology of the People's Republic of China (No. 2011CB932604), and the Education Department of Sichuan Province (No. 13ZB0205).

References

[1] S.W. Han, J.H. Ryu, J. Jeong, D.H. Yoon, J. Alloys Comp. 570 (2013) 144–149.
[2] F. Ning, Y.B. He, B.H. Li, H.D. Du, D.Y. Zhai, F.Y. Kang, J. Alloys Comp. 513 (2012) 524–529.
[3] C.Y. Lin, J.G. Duh, J. Alloys Comp. 509 (2011) 3682–3685.
[4] F.X. Wu, Z.X. Wang, X.H. Li, L. Wu, X.J. Wang, X.P. Zhang, Z.G. Wang, X.H. Xiong, H.J. Guo, J. Alloys Comp. 509 (2011) 596–601.
[5] Z.J. He, Z.X. Wang, F.X. Wu, H.J. Guo, X.H. Li, X.H. Xiong, J. Alloys Comp. 540 (2012) 39–45.
[6] S.H. Ju, Y.C. Kang, J. Alloys Comp. 506 (2010) 913–916.
[7] G.Q. Liu, L. Wen, G.Y. Liu, Q.Y. Wu, H.Z. Luo, B.Y. Ma, Y.W. Tian, J. Alloys Comp. 509 (2011) 6427–6432.
[8] T. Yuan, R. Cai, R. Ran, Y.K. Zhou, Z.P. Shao, J. Alloys Comp. 505 (2010) 367–373.
[9] T.F. Yi, B. Chen, H.Y. Shen, R.S. Zhu, A.N. Zhou, H.B. Qiao, J. Alloys Comp. 558 (2013) 11–17.
[10] L. Zhao, Y.S. Hu, H. Li, Z.X. Wang, L.Q. Chen, Adv. Mater. 23 (2011) 1385–1388.
[11] C.T. Hsieh, J.Y. Lin, J. Alloys Comp. 506 (2010) 231–236.
[12] C.Y. Lin, Y.R. Jhan, J.G. Duh, J. Alloys Comp. 509 (2011) 6965–6968.
[13] C.T. Hsieh, B.S. Chang, J.Y. Lin, R.S. Juang, J. Alloys Comp. 513 (2012) 393–398.
[14] J. Wang, L. Shen, H. Li, B. Ding, P. Nie, H. Dou, X. Zhang, J. Alloys Comp. 587 (2014) 171–176.
[15] B. Wang, J. Cao, Y. Liu, T. Zeng, L. Li, J. Alloys Comp. (2013) (http://dx.doi.org/10.1016/j.jallcom.2013.10.167).
[16] Y.R. Zhu, L.C. Yin, T.F. Yi, H.P. Liu, Y. Xie, R.S. Zhu, J. Alloys Comp. 547 (2013) 107–112.
[17] G.Y. Liu, H.Y. Wang, G.Q. Liu, Z.Z. Yang, B. Jin, Q.C. Jiang, Electrochim. Acta 87 (2013) 218–223.
[18] J. Mosa, J.F. Vélez, J.J. Reinosa, M. Aparicio, A. Yamaguchi, K. Tadanaga, M. Tatsumisago, J. Power Sources 244 (2013) 482–487.
[19] W.L. Zhang, J.F. Li, Y.B. Guan, Y. Jin, W.T. Zhu, X. Guo, X.P. Qiu, J. Power Sources 243 (2013) 661–667.
[20] L. Sun, J.P. Wang, K.L. Jiang, S.S. Fan, J. Power Sources 248 (2014) 265–272.
[21] L.J. Xi, H.K. Wang, S.L. Yang, R.G. Ma, Z.G. Lu, C.W. Cao, K.L. Leung, J.Q. Deng, A.L. Rogach, C.Y. Chung, J. Power Sources 242 (2013) 222–229.
[22] X.R. Li, H. Hu, S. Huang, G.G. Yu, L. Gao, H.W. Liu, Y. Yu, Electrochim. Acta 112 (2013) 356–363.
[23] Q.Y. Zhang, C.L. Zhang, B. Li, S.F. Kang, X. Li, Y.G. Wang, Electrochim. Acta 98 (2013) 146–152.
[24] W. Xu, X.L. Chen, W. Wang, D.W. Choi, F. Ding, J.M. Zheng, Z.M. Nie, Y.J. Choi, J.G. Zhang, Z.G. Yang, J. Power Sources 236 (2013) 169–174.
[25] J.S. Park, S.H. Baek, Y.Il. Jeong, B.Y. Noh, J.H. Kim, J. Power Sources 244 (2013) 527–531.
[26] C.F. Lin, M.O. Lai, L. Lu, H.H. Zhou, Y.L. Xin, J. Power Sources 244 (2013) 272–279.
[27] Q.Y. Zhang, C.L. Zhang, B. Li, D.D. Jiang, S.F. Kang, X. Li, Y.G. Wang, Electrochim. Acta 107 (2013) 139–146.
[28] Z. Zhao, Y.L. Xu, M.J. Ji, H. Zhang, Electrochim. Acta 109 (2013) 645–650.
[29] M. Krajewski, M. Michalska, B. Hamankiewicz, D. Ziolkowska, K.P. Korona, J.B. Jasinski, M. Kaminska, L. Lipinska, A. Czerwinski, J. Power Sources 245 (2014) 764–771.
[30] W. Wang, Y.Y. Guo, L.X. Liu, S.X. Wang, X.J. Yang, H. Guo, J. Power Sources 245 (2014) 624–629.
[31] H.J. Luo, L.F. Shen, K. Rui, H.S. Li, X.G. Zhang, J. Alloys Comp. 572 (2013) 37–42.

[32] J. Wang, X.M. Liu, H. Yang, X.D. Shen, J. Alloys Comp. 509 (2011) 712–718.
[33] X.B. Hu, Z.J. Lin, K.R. Yang, Z.H. Deng, J.S. Suo, J. Alloys Comp. 506 (2010) 160–166.
[34] Y.H. Yin, S.Y. Li, Z.X. Cao, H.Y. Yue, X.L. Ding, S.T. Yang, Solid State Ionics 241 (2013) 1–4.
[35] W. Fang, X.Q. Cheng, P.J. Zuo, Y.L. Ma, G.P. Yin, Electrochim. Acta 93 (2013) 173–178.
[36] Y. Wang, H.B. Rong, B.Z. Li, L.D. Xing, X.P. Li, W.S. Li, J. Power Sources 246 (2014) 213–218.
[37] G.L. Yang, Z. Su, H.S. Fang, Y.C. Yao, Y.M. Li, B. Yang, W.H. Ma, Electrochim. Acta 93 (2013) 158–162.
[38] H.G. Jung, N. Venugopal, B. Scrosati, Y.K. Sun, J. Power Sources 221 (2013) 266–271.
[39] H.S. Li, L.F. Shen, X.G. Zhang, J. Wang, P. Nie, Q. Che, B. Ding, J. Power Sources 221 (2013) 122–127.
[40] Y. Ding, G.R. Li, C.W. Xiao, X.P. Gao, Electrochim. Acta 102 (2013) 282–289.
[41] H.F. Xiang, B.B. Tian, P.C. Lian, Z. Li, H.H. Wang, J. Alloys Comp. 509 (2011) 7205–7209.
[42] X. Guo, H.F. Xiang, T.P. Zhou, W.H. Li, X.W. Wang, J.X. Zhou, Y. Yu, Electrochim. Acta 109 (2013) 33–38.
[43] S.G. Ri, L. Zhan, Y. Wang, L.H. Zhou, J. Hu, H.L. Liu, Electrochim. Acta 109 (2013) 389–394.
[44] Q. Zhang, W.J. Peng, Z.X. Wang, X.H. Li, X.H. Xiong, H.J. Guo, Z.G. Wang, F.X. Wu, Solid State Ionics 236 (2013) 30–36.
[45] S.P. Pang, Y.Y. Zhao, C.J. Zhang, Q.H. Zhang, L. Gu, X.H. Zhou, G.C. Li, G.L. Cui, Scripta Mater. 69 (2013) 171–174.
[46] X. Li, M.Z. Qu, Z.L. Yu, J. Alloys Comp. 487 (2009) L12–L17.
[47] F.X. Wu, X.H. Li, Z.X. Wang, H.J. Guo, Z.J. He, Q. Zhang, X.H. Xiong, P. Yue, J. Power Sources 202 (2012) 374–379.
[48] T.F. Yi, Y. Xie, L.J. Jiang, J. Shu, C.B. Yue, A.N. Zhou, M.F. Ye, RSC Advances 2 (2012) 3541–3547.
[49] X.L. Yao, S. Xie, H.Q. Nian, C.H. Chen, J. Alloys Comp. 465 (2008) 375–379.
[50] S.H. Ju, Y.C. Kang, J. Power Sources 195 (2010) 4327–4331.
[51] H. Ge, N. Li, D.Y. Li, C.S. Dai, D.L. Wang, Electrochem. Commun. 10 (2008) 719–722.
[52] Y.B. He, F. Ning, B.H. Li, Q.S. Song, W. Lv, H.D. Du, D.Y. Zhai, F.Y. Su, Q.H. Yang, F.Y. Kang, J. Power Sources 202 (2012) 253–261.
[53] Y.B. He, B.H. Li, M. Liu, C. Zhang, W. Lv, C. Yang, J. Li, H.D. Du, B. Zhang, Q.H. Yang, J.K. Kim, F.Y. Kang, Sci. Rep. 2 (913) (2012) 1–7.